Missing-in-metastasis MIM/MTSS1 promotes actin assembly at intercellular junctions and is required for integrity of kidney epithelia

Juha Saarikangas[1,*], Pieta K. Mattila[1,*,‡], Markku Varjosalo[2], Miia Bovellan[1], Janne Hakanen[3], Julia Calzada-Wack[4], Monica Tost[4], Luise Jennen[4], Birgit Rathkolb[5,6], Wolfgang Hans[6], Marion Horsch[6], Mervi E. Hyvönen[7], Nina Perälä[2], Helmut Fuchs[5], Valérie Gailus-Durner[5], Irene Esposito[4], Eckhard Wolf[6], Martin Hrabé de Angelis[5,8], Mikko J. Frilander[1], Harri Savilahti[1,9], Hannu Sariola[2], Kirsi Sainio[2], Sanna Lehtonen[7], Jussi Taipale[2], Marjo Salminen[3] and Pekka Lappalainen[1,§]

[1]Institute of Biotechnology, P.O. Box 56, University of Helsinki, 00014 Finland
[2]Institute of Biomedicine, P.O. Box 63, University of Helsinki, 00014 Finland
[3]Department of Basic Veterinary Sciences, P.O. Box 66, University of Helsinki, 00014 Finland
[4]Institute of Pathology, Helmholtz Zentrum München, German Research Center for Environmental Health, 85764 Neuherberg, Germany
[5]Institute of Experimental Genetics, Helmholtz Zentrum München, German Research Center for Environmental Health, 85764 Neuherberg, Germany
[6]Chair of Molecular Animal Breeding and Biotechnology, Gene Center, Ludwig-Maximilians-Universität München, 81377 Munich, Germany
[7]Haartman Institute, Department of Pathology, P.O. Box 21, University of Helsinki, 00014 Finland
[8]Lehrstuhl für Experimentelle Genetik, Technische Universität München, 85350 Freising-Weihenstephan, Germany
[9]Division of Genetics and Physiology, Department of Biology, University of Turku, 20014 Turku, Finland

*These authors contributed equally to this work
‡Present address: Cancer Research UK London Research Institute, 44 Lincoln's Inn Fields, London WC2A 3PX, UK
§Author for correspondence (pekka.lappalainen@helsinki.fi)

Accepted 29 November 2010
Journal of Cell Science 124, 1245-1255

doi:10.1242/jcs.082610

Summary

MIM/MTSS1 is a tissue-specific regulator of plasma membrane dynamics, whose altered expression levels have been linked to cancer metastasis. MIM deforms phosphoinositide-rich membranes through its I-BAR domain and interacts with actin monomers through its WH2 domain. Recent work proposed that MIM also potentiates Sonic hedgehog (Shh)-induced gene expression. Here, we generated MIM mutant mice and found that full-length MIM protein is dispensable for embryonic development. However, MIM-deficient mice displayed a severe urinary concentration defect caused by compromised integrity of kidney epithelia intercellular junctions, which led to bone abnormalities and end-stage renal failure. In cultured kidney epithelial (MDCK) cells, MIM displayed dynamic localization to adherens junctions, where it promoted Arp2/3-mediated actin filament assembly. This activity was dependent on the ability of MIM to interact with both membranes and actin monomers. Furthermore, results from the mouse model and cell culture experiments suggest that full-length MIM is not crucial for Shh signaling, at least during embryogenesis. Collectively, these data demonstrate that MIM modulates interplay between the actin cytoskeleton and plasma membrane to promote the maintenance of intercellular contacts in kidney epithelia.

Key words: I-BAR, Actin, Knockout mouse, Cadherin, Sonic hedgehog, EMT, Phosphoinositide

Introduction

The actin cytoskeleton is a key regulator of cell morphology and migration. Consequently, it is crucial for embryonic development and many physiological functions in adult animals. Abnormalities in the function of the actin cytoskeleton are also central in cancer, and many actin-binding proteins have been directly linked to the metastatic behavior of cancer cells (Wang, W. et al., 2007a).

Processes mediated by the actin cytoskeleton, such as the formation of plasma membrane protrusions during cell migration, are often closely linked to direct membrane remodeling (Chhabra and Higgs, 2007). Recent studies demonstrated that the members of an extended protein family, characterized by the presence of a membrane binding and deforming BAR (Bin–Amphiphysin–Rvs) domain, function at the interface between the actin cytoskeleton and plasma membrane during the formation of membrane protrusions or invaginations (Doherty and McMahon, 2008; Frost et al., 2009; Itoh et al., 2005; Peter et al., 2004; Takano et al., 2008). These proteins can either generate positive membrane curvature to facilitate the formation of plasma membrane invaginations (e.g. BAR, N-BAR and F-BAR domain proteins) or induce negative membrane curvature to promote the formation of plasma membrane protrusions (I-BAR and IF-BAR domain proteins) (Guerrier et al., 2009; Mattila et al., 2007; Suetsugu et al., 2006).

Missing-in-metastasis (MIM/MTSS1), an actin and membrane binding protein, was first identified as a tumor suppressor, which is downregulated in bladder carcinoma cell lines with increased metastatic potential (Lee et al., 2002). Subsequent studies also demonstrated decreased expression of MIM in other cancer types (Ma et al., 2007; Wang, Y. et al., 2007a). In mice, MIM is expressed specifically in a few embryonic cell types, such as muscle and post-mitotic neurons, as well as in adult kidney, liver and Purkinje cells of the cerebellum (Machesky and Johnston, 2007; Mattila et al., 2003). MIM is composed of a C-terminal actin-monomer-

Journal of Cell Science

binding WH2 (WASP homology 2) domain and an N-terminal I-BAR (inverse BAR) domain, also known as an IRSp53/MIM homology domain (IMD) (Mattila et al., 2003; Woodings et al., 2003; Yamagishi et al., 2004). The I-BAR domain was originally proposed to bundle actin filaments and thus induce the formation of filopodia-like plasma membrane protrusions when expressed in cells (Yamagishi et al., 2004). However, subsequent studies revealed that the I-BAR domain does not display significant actin filament bundling activity under physiological conditions, but rather binds to membranes rich in phosphatidylinositol (4,5)-bisphosphate [PtdIns(4,5)P_2], which it then deforms into tubular structures *in vitro* (Lee et al., 2007; Mattila et al., 2007; Saarikangas et al., 2009; Suetsugu et al., 2006). Interestingly, MIM was recently also implicated in the Sonic hedgehog (Shh) signaling pathway. Shh is a potent morphogen that controls many developmental processes, including left–right asymmetry and organ patterning. Ectopic or dysfunctional Shh signaling has been linked to many cancers (Varjosalo and Taipale, 2008). MIM was characterized as a Shh-responsive gene in both normal tissues and basal cell carcinomas, and was proposed to enhance Gli-mediated transcription through direct interactions with Gli1 and Gli2 transcription factors and by antagonizing Src-dependent phosphorylation of cortactin to regulate ciliogenesis (Callahan et al., 2004; Gonzalez-Quevedo et al., 2005; Bershteyn et al., 2010). This provided a plausible explanation for the correlation between MIM expression levels and metastatic potential of certain cancer types.

Despite the wealth of biochemical data, the physiological roles of MIM and its various activities (actin monomer binding, membrane deformation, Gli-mediated transcription) have not been reported. By inactivating the mouse *Mim/Mtss1* gene, we demonstrate that full-length MIM protein is dispensable for embryonic development and Shh signaling. In adult mice, MIM deficiency leads to a progressive kidney disease characterized by abnormal tubular morphology, severe urine concentration defects, renal electrolyte wasting and bone abnormalities. These data, together with cell biological analysis of MIM localization and dynamics in MDCK cells, propose that MIM interacts with phosphoinositide-rich membranes and monomeric actin to modulate Arp2/3-mediated actin polymerization, and thus contributes to the integrity of cell–cell contacts in epithelia.

Results

MIM is dispensable for embryonic development

To analyze the physiological functions of MIM, we inactivated the mouse *Mim* gene by inserting a Neomycin (Neo) gene cassette, which contains several translation stop codons, into exon 1 (Fig. 1A). The successful gene targeting was verified by Southern blotting on genomic DNA from the targeted mouse embryonic stem (ES) cells (Fig. 1B). In-frame stop codons present in the targeting cassette are expected to destabilize the MIM transcript via the nonsense-mediated decay (NMD) pathway. Consistently, tissues from mice homozygous for MIM mutation ($Mim^{-/-}$) expressed only very low levels of *Mim* mRNA fragments as verified by qRT-PCR and RNA in situ hybridization (Fig. 1C,D). Furthermore, the lack of full-length MIM protein was confirmed by western blot analysis using an anti-MIM antibody (Fig. 1E,F).

Although our $Mim^{-/-}$ mice do not express full-length MIM, it is important to note that another EST transcript is also associated with the *Mim* genomic locus. This shorter transcript contains an alternative 5′ exon, which is probably associated with an alternative promoter that is located in the intron 3 of the *Mim* gene. Thus, it can bypass our targeting construct and could possibly be translated to a protein lacking the first 81 residues of MIM, resulting in an I-BAR domain that lacks the membrane insertion motif, as well as a large part of the dimerization interfaces (supplementary material Fig. S1A–C). RT-PCR analysis revealed that this transcript is present in a subset of organs expressing MIM and is also found in the targeted MIM mutant mice (supplementary material Fig. S1D and data not shown). Importantly, our cell biological analysis revealed that the N-terminal I-BAR domain, which is crucial for the cellular role of MIM, is non-functional in the putative truncated protein and cannot deform membranes. Furthermore, the protein corresponding to the shorter transcript does not localize correctly to the plasma membrane when expressed in cells (supplementary material Fig. S1E,F). These data show that, if this transcript is indeed translated into a protein, it cannot promote membrane dynamics in cells. Thus, the MIM mutant mice generated and analyzed here do not express functional MIM protein that is capable of binding/deforming PtdIns(4,5)P_2-rich membranes.

The heterozygous MIM ($Mim^{+/-}$) mice were phenotypically normal and fertile. Their inter-crosses resulted in $Mim^{-/-}$ mice at expected mendelian ratios. The MIM mutant mice survived into adulthood and had normal appearance and bodyweight (Fig. 1G and Fig. 2A). A detailed morphological inspection and histological analysis of all major organs was carried out on 2- to 3-month-old animals and did not reveal any gross abnormalities in $Mim^{-/-}$ mice.

The mammalian IRSp53/MIM protein family, characterized by the N-terminal I-BAR domain, consists of five members and is divided in two branches (Scita et al., 2008). The first consists of MIM and ABBA, which show high sequence similarity within I-BAR and WH2 domains, but differ in the middle region, conceivably indicating divergence in the function. The tissue distributions of ABBA and MIM in embryonic and adult mice are mainly distinct (Saarikangas et al., 2008). Accordingly, the tissue distribution of ABBA was not changed in MIM mutant mice, suggesting that ABBA cannot compensate for the lack of MIM (supplementary material Fig. S2). The expression patterns of the three more distantly related I-BAR proteins, IRSp53, IRTKS and FLJ22582, are less well characterized, and it is thus possible that some of them might have partially redundant functions with MIM.

Full-length MIM is not required for Shh signaling in mice or cultured cells

The Shh signaling pathway is indispensable for embryonic development, but the MIM-deficient mice showed no abnormalities in embryonic development or in the morphology of teeth, skull and hairs, which are ectodermal organs regulated by Shh during embryogenesis (Varjosalo and Taipale, 2008). Thus, we readdressed the suggested role of MIM in Shh signaling (Callahan et al., 2004; Bershteyn et al., 2010).

Cellular responses to Shh are transmitted through its receptor Patched (Ptc), which upon ligand binding, releases the repression of Smoothened, and activates signal transduction, ultimately leading to activation of Gli transcription factors (Varjosalo and Taipale, 2008). In Ptc-knockout ($Ptch1^{-/-}$) mice, Shh signaling is constitutively active causing embryonic lethality at E9–E10.5, probably because of abnormal development of the heart. Additionally, these embryos display a neural tube closure defect and are severely malformed (Goodrich et al., 1997). We crossed $Mim^{-/-}$ mice with $Ptch1^{+/-}$ mice to create double targeted mice. Loss of protein that activates Gli should reduce Shh-dependent transcription, which can be monitored by the expression of the

marker gene β-galactosidase (β-gal) in the *Ptch1*$^{-/-}$ mouse strain. However, similar high levels of β-gal expression were observed in both *Ptch1*$^{-/-}$ and *Mim*$^{-/-}$ *Ptch1*$^{-/-}$ embryos indicating that loss of MIM did not decrease Gli activity (supplementary material Fig. S3A). Furthermore, if MIM was an activator of Gli1 or Gli2, loss of MIM should partially rescue the *Ptch1*$^{-/-}$ phenotype by lowering the activity of Shh-dependent transcription in organs where both proteins are functioning. Because MIM is also highly expressed in the developing central nervous system and heart (Mattila et al., 2003), the phenotypes of *Ptch1*$^{-/-}$ embryos should be at least partially rescued in double-knockout embryos (see Bai et al., 2002). However, comparative analysis between *Ptch1*$^{-/-}$ and *Mim*$^{-/-}$ *Ptch1*$^{-/-}$ embryos revealed that the lack of MIM did not rescue the phenotype of *Ptch1*$^{-/-}$ embryos to any detectable level, with no improvement in the morphology or survival of the embryos (supplementary material Fig. S3A). These data suggest that full-length MIM is not crucial for Shh signaling, at least during embryogenesis.

To exclude the possibility that putative shorter versions of MIM protein, which might be expressed in our MIM-deficient mice, could contribute to Shh signaling, we reassessed the role of MIM in Gli-mediated transcription by carrying out a Shh reporter assay in a NIH3T3 cell culture model. Here, we used corresponding constructs to the ones applied in the previous study concerning the role of MIM in Gli-dependent transcription (Callahan et al., 2004). In this Hedgehog-pathway-specific signaling assay, a firefly luciferase gene is under the control of a Gli-specific promoter (Taipale et al., 2000). This assay did not reveal any effect of MIM or ABBA in transcription by either endogenous Gli transcription factors induced by Shh or when MIM was co-expressed with Gli1 or Gli2 (supplementary material Fig. S3B and data not shown). Additionally, in contrast to the previous study (Callahan et al.,

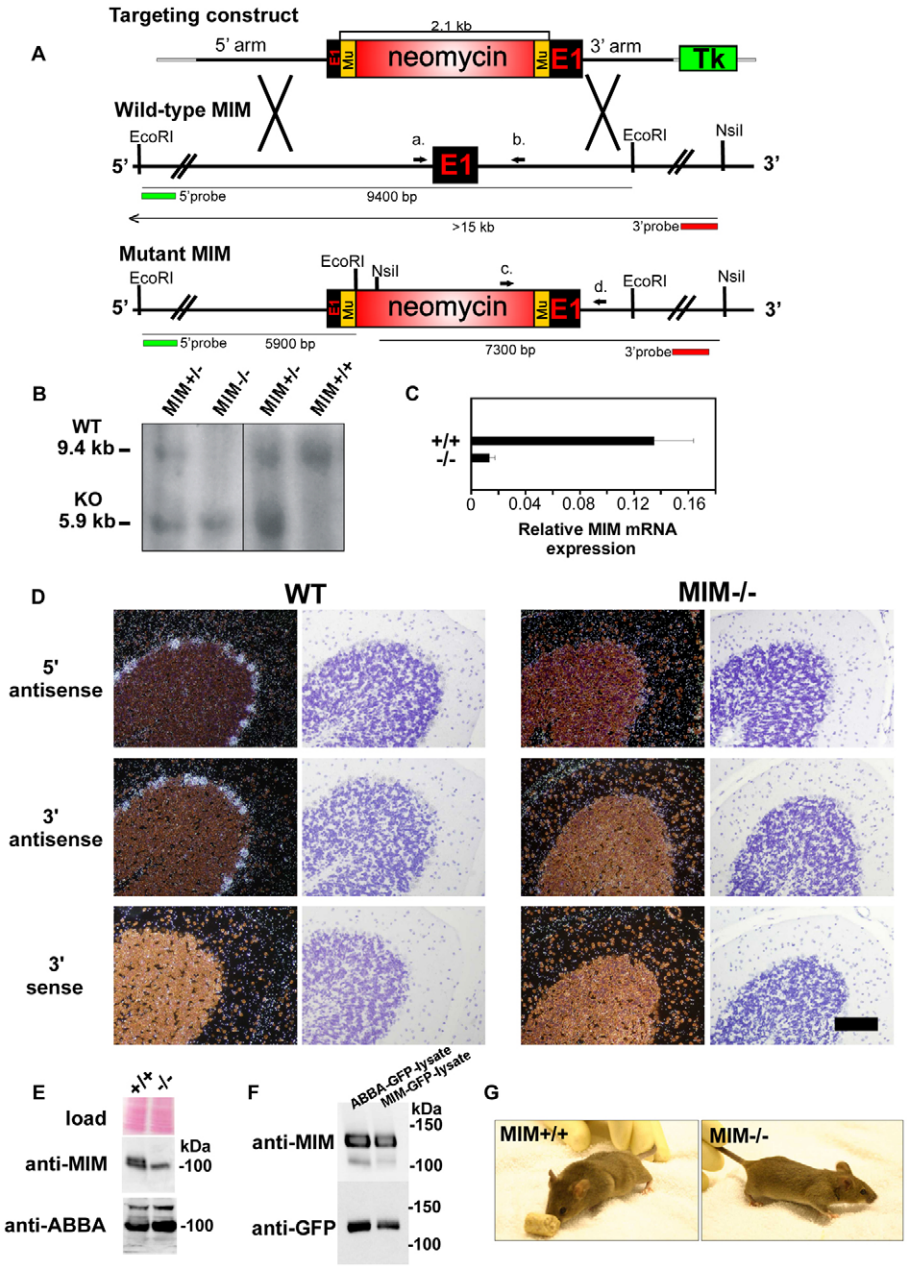

Fig. 1. Generation of MIM mutant mice. (**A**) The mouse *Mim* gene was interrupted by the insertion of a Neo cassette by Mu transposition into the first exon. TK, thymidine kinase. (**B**) Successful gene targeting was verified with Southern blot analysis of the genomic DNA. (**C**) Lack of *Mim* transcripts in *Mim*$^{-/-}$ mouse tissues was verified by qRT-PCR analysis of total RNA isolated from kidney. Graph indicates the ratio of *Mim* to *Gapdh*, which was used as a reference. (**D**) RNA in situ hybridization analysis using 5′ and 3′ probes on sections through adult *Mim*$^{+/+}$ mouse brain show strong MIM expression in cerebellar Purkinje cells, whereas no MIM expression is detected in *Mim*$^{-/-}$ cerebellum, demonstrating lack of MIM transcript. Scale bar: 100 µm. (**E**) Western blot analysis of MIM and ABBA proteins in wild-type and *Mim*$^{-/-}$ mice cerebellar lysates. This assay demonstrates the absence of a band of expected electrophoretic motility from *Mim*$^{-/-}$ cerebellar lysate, whereas ABBA protein levels are not affected in *Mim*$^{-/-}$ mice. Ponceau staining is shown as a loading control. (**F**) The residual ~100 kDa band in *Mim*$^{-/-}$ lysates probably represents ABBA because the anti-MIM (P549) antibody crossreacts with ABBA. In this experiment GFP–MIM and GFP–ABBA were expressed in U2OS cells and the fusion proteins were detected from western blots using antibodies against MIM (P549) and GFP. (**G**) MIM mutant mice develop normally into adulthood and do not display any gross abnormalities.

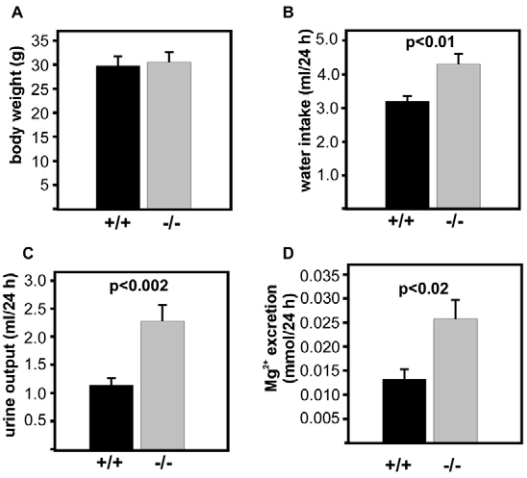

Fig. 2. MIM mutant mice display a severe urinary-concentration defect. (**A**) Body weight of *Mim*$^{-/-}$ mice is similar to that of wild-type littermates (+/+) at the age of 8 months. (**B**,**C**) The water consumption and urinary output over 24 hours measured for mice maintained in metabolic cages is significantly increased in MIM-knockout mice. (**D**) Excretion of Mg^{2+} through the urine over 24-hours is increased in the *Mim*-null mice. Error bars represent s.e.m. Student's *t*-test was used for statistical measurements. Ten mice per genotype were tested.

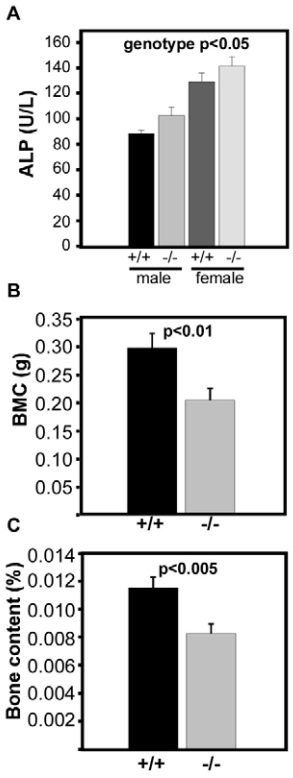

Fig. 3. MIM mutants display altered bone metabolism. (**A**) Plasma alkaline phosphatase (ALP) activity is significantly (P<0.05, ANOVA) increased in *Mim*$^{-/-}$ mice, indicating higher bone turnover rate (n=20 mice per genotype). (**B**,**C**) Dual-energy X-ray absorptiometry revealed that bone mineral content (BMC) and bone content are significantly decreased in *Mim*$^{-/-}$ mice. P<0.01 and P<0.005, Student's *t*-test (n=20 mice per genotype). Error bars represent s.e.m.

2004), Gli1 and Gli2 failed to interact with MIM–GFP in co-immunoprecipitation experiments (supplementary material Fig. S3C). Taken together, we found no evidence that full-length MIM has a crucial role in Shh-dependent transcription. However, based on this experimental system, we cannot definitely rule out a possible minor role of MIM in Shh-mediated transcription or its function in ciliogenesis in other cell-types, as suggested recently (Bershteyn et al., 2010).

Lack of MIM leads to polyuria, renal electrolyte wasting and altered bone metabolism

In adult mice, MIM is strongly expressed in the kidney cortex (Mattila et al., 2003) (supplementary material Fig. S4C). To analyze the renal functions of MIM mice, we applied metabolic cages to collect 24-hour urine samples from 8-month-old wild-type and *Mim*$^{-/-}$ littermates (n=10 per genotype). Urine analysis revealed alterations in several parameters. First, *Mim*-null mice displayed significantly higher water intake (P<0.01, Student's *t*-test) and urine production (P<0.002) compared with that in wild-type littermates (Fig. 2B,C). In addition, urinary wasting of electrolyte Mg^{2+} (P<0.02) over 24 hours was increased (Fig. 2D). Similarly, urinary wasting of Ca^{2+}, K^{+} and Na^{+} was increased, although these changes were not statistically significant (data not shown). These results suggest that *Mim*$^{-/-}$ mice suffer from reduced tubular water and electrolyte absorption in the kidney.

Alterations in bone metabolism are common in patients with chronic kidney disease (Magnusson et al., 2001) and were previously reported for mouse models with polyuria and renal electrolyte wasting (Hoenderop et al., 2003; Hou et al., 2007). A clinical chemistry screen revealed significantly increased plasma alkaline phosphatase (ALP) levels in *Mim*-null mice (P<0.05, one-way ANOVA), suggesting that they have a higher bone turnover rate compared with wild-type mice (Fig. 3A). Plasma ALP is considered a good marker for measuring bone metabolism in patients with renal disease because it is not influenced by variations in renal function (Magnusson et al., 2001).

Bone densitometry using dual-energy X-ray absorptiometry (DXA) revealed that both bone mineral content (BMC) (P<0.01) and bone content (P<0.005) were significantly decreased in MIM mutants (n=20 per genotype) when compared with wild-type littermates (Fig. 3B,C), and this phenotype was more pronounced in females. The observed changes cannot be explained by differences in body weight or bone length. We propose that the differences observed in the bone represent a secondary effect of the kidney defect (e.g. altered Ca^{2+} homeostasis).

MIM is necessary for the maintenance of intercellular junctions in kidney epithelia

Although no morphological or histological abnormalities were detected in the kidneys of 2- to 5-month-old MIM mice (Fig. 4A,B), many *Mim*$^{-/-}$ mice became sick and died at around 8–18 months. Detailed histological analysis revealed dramatic changes in the kidney histology (Fig. 4C–F). Based on the observed pathological changes, the progression of the kidney disease in *Mim*$^{-/-}$ mice was categorized into three stages. At stage I of the disease, dilated tubular structures were observed, and this was followed by infiltration of lymphocytes together with

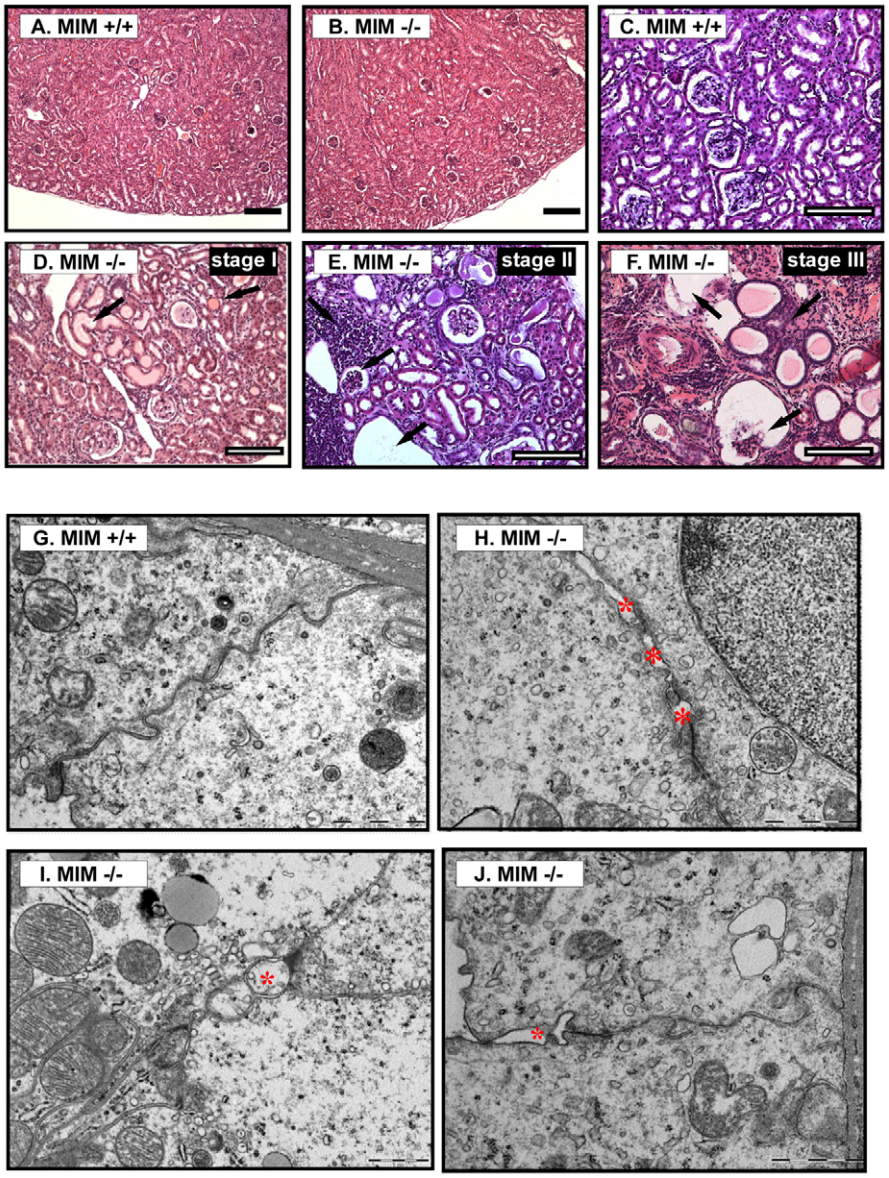

Fig. 4. The kidney proximal tubules of MIM mutant mice display irregular intercellular junctions. (**A**,**B**) Hematoxylin and eosin stained sections of 5-month-old $Mim^{-/-}$ mouse kidneys show no histological alterations compared with $Mim^{+/+}$ mouse kidneys. Representative images from kidney sections of 17-month-old (**C**) $Mim^{+/+}$and (**D**) $Mim^{-/-}$ mice, which shows the first signs of the kidney disease (stage I) with tubular dilation (arrows in D). Kidneys of $Mim^{+/+}$ appear normal. (**E**,**F**) Representative images of $Mim^{-/-}$ kidneys that display more severe (stage II) kidney disease with dilation of kidney tubules, degeneration of the glomeruli and lymphocyte infiltration (arrows), and finally (stage III), also massive interstitial fibrosis and loss of glomeruli (arrows). Scale bars: 100 µm. (**G**–**J**) TEM images from proximal tubule intercellular junctions. In wild-type mice, the intercellular junctions are uniform (G), whereas in MIM mutant mice (H-J) the intercellular junctions are widened in an irregular fashion (indicated by red asterisks). Scale bars: 1 µm.

glomerulosclerosis (stage II). At the end stage of the disease, massive fibrosis together with glomerular degeneration was observed (stage III). The onset of the first histological signs of the renal disease varied widely between individuals. Some histologically abnormal kidneys were also detected in aged wild-type littermates, but with much milder anomalies compared with those in $Mim^{-/-}$ mice.

To assess the detailed primary changes in $Mim^{-/-}$ mice, we analyzed the kidney ultrastructures of three mice per genotype using transmission electron microscopy (TEM). The selected $Mim^{-/-}$ mice displayed polyuria, but appeared otherwise normal (with normal body weight) and therefore were concluded to represent an early stage of the kidney disease. Interestingly, TEM analysis revealed apparent atrophic changes in the ultrastructure of the renal proximal tubules of the mutant mice, whereas such abnormalities were not observed in the control wild-type littermates. Dilated lateral intercellular spaces at the cell–cell contacts were observed in $Mim^{-/-}$ mice (Fig. 4G–J). Furthermore, thickening of the basement membrane was detected in *Mim*-deficient mice but not in control mice (supplementary material Fig. S5). The lateral intercellular space represents a pathway for fluid and ion transport, and the observed changes in the ultrastructure of $Mim^{-/-}$ kidneys are thus consistent with polyuria and renal electrolyte wasting in these mice. It is also important to note that EM analysis did not reveal alterations in the density or morphology of brush border in kidney proximal tubules (data not shown).

We also conducted immunohistochemical analysis using a tight junction marker (ZO-1), F-actin, Arp2/3 complex and glomerular markers (nephrin, synaptopodin, podocin and CD2AP) at the early stages of the disease. No apparent changes in the distribution or signal intensity between wild-type and MIM mutant mice were detected (supplementary material Figs S6 and S7). In addition, an RNA expression profiling analysis did not reveal differentially expressed genes in the kidneys of young $Mim^{-/-}$ and wild-type mice (additional materials and methods; please contact the author for further information).

Similar ultrastructural changes in the kidney epithelia leading to polyuria and electrolyte wasting as described here for $Mim^{-/-}$ mice

were previously detected in mice lacking tight junction component claudin-16, as well as in humans suffering from cystic kidney disease nephronophthisis and kaliopenic nephropathy (Hou et al., 2007; Krishnan et al., 2008; Simon et al., 1999; Wang, W. et al., 2007b). This suggests that defects in cell–cell contacts compromising epithelial integrity can reduce osmotic gradient for effective water reabsorption or might result in backflow of water through the junctional space, and thus lead to polyuria. It is important to note that at early stages of kidney disease, no specific abnormalities were detected in the glomeruli of *Mim*$^{-/-}$ mice, suggesting that the observed phenotype originates from kidney tubules. Moreover, no systematic proteinuria was detected in *Mim*-null mice, indicating that glomerular failure is probably not the primary cause of the symptoms.

Together, these data imply that MIM is not essential for the formation of cell–cell contacts in kidney epithelium, but instead contributes to their maintenance. It is important to note that the I-BAR protein IRSp53 is also expressed in kidney (supplementary material Fig. S4B,D). Interestingly, a recent study suggested that IRSp53 contributes to the formation or maintenance of tight junctions in cultured Madin-Darby canine kidney (MDCK) cells (Massari et al., 2009). Thus, I-BAR domain proteins appear to have an important, but probably at least partially redundant, role in the maintenance of specialized cell adhesion structures in the kidney epithelium.

MIM promotes actin and membrane dynamics at adherens junctions of cultured MDCK cells

Previous studies demonstrated that overexpression of MIM induces the formation of filopodia, microspikes and membrane ruffles in cultured mammalian cells (Bompard et al., 2005; Lin et al., 2005; Mattila et al., 2003; Woodings et al., 2003; Yamagishi et al., 2004). However, the subcellular localization, dynamics and role of MIM in confluent epithelial cells have not been reported. We used MDCK cell line to examine the localization of MIM in kidney epithelial cells. In the absence of a good antibody for immunofluorescence microscopy, MIM localization in polarized monolayer of MDCK cells was examined by using a MIM–GFP construct. Interestingly, in MDCK cells MIM localized to the plasma membrane and was strongly enriched at cell–cell adhesions, where it colocalized with F-actin and the adherens junction marker E-cadherin. Small amounts of MIM were also detected at tight junctions (Fig. 5A–C). Importantly, inactivation of the membrane binding and deforming I-BAR domain by previously characterized point mutations abolished the localization of MIM to cell–cell adhesions and plasma membrane, whereas inactivation of the actin-binding WH2 domain had no detectable effect on the subcellular localization of MIM (Fig. 5D,E). Fluorescence recovery after photobleaching (FRAP) analysis revealed that GFP–MIM localization to the cell–cell contacts was highly dynamic, with a $t_{1/2}$ of ~7 seconds (Fig. 6A,B). Together, these results demonstrate that in cultured kidney epithelial cells, MIM displays dynamic localization to cell–cell adhesions through its membrane binding and deforming I-BAR domain.

To elucidate the mechanism by which MIM is recruited to cell–cell contacts, we engineered a construct expressing a hybrid MIM protein. In this construct, the phosphoinositide binding of the I-BAR was inactivated by point mutations (see above), and the protein was fused to a PtdIns(4,5)P_2-specific PH domain from the N-terminus of PLCδ (Varnai and Balla, 1998). Thus, in the hybrid protein, the PtdIns(4,5)P_2-binding activity of the I-BAR domain was replaced by a PtdIns(4,5)P_2-binding PH domain without

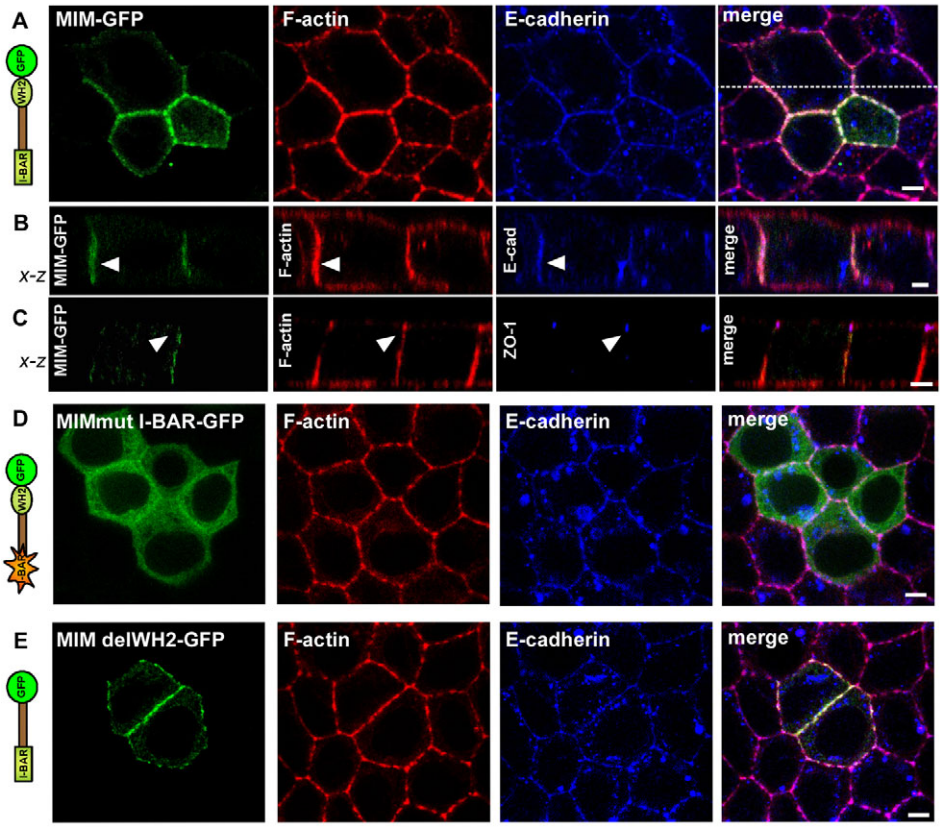

Fig. 5. MIM localizes to intercellular junctions in cultured MDCK epithelial cells. (**A**) Polarized MDCK cells form cell–cell contacts that are enriched with GFP-tagged wild-type MIM, E-cadherin and F-actin. (**B**) Confocal *z*-stack analysis from the indicated area from panel A demonstrates that MIM colocalizes at adherens junctions with E-cadherin and F-actin (arrowhead). (**C**) MIM does not concentrate at tight junctions located at the most apical part of the intercellular contact that are indicated by ZO-1 staining (arrowhead). (**D**) Localization of MIM to intercellular junctions is disrupted when the membrane binding by I-BAR domain is inactivated by point mutations. (**E**) Deletion of the actin- monomer-binding WH2 domain has no effect on localization of MIM to the intercellular contacts. Scale bars: 4 µm (A,B,D,E), 3 µm (C).

affecting the overall structure or dimerization properties of MIM or its I-BAR domain. Interestingly, whereas the wild-type GFP–MIM preferentially localized to intercellular junctions when expressed in MDCK cells, the chimeric MIM-PH protein displayed a more uniform plasma membrane localization to both lateral and apical regions of the cells (Fig. 6C,D).

To understand the possible role of MIM in actin and plasma membrane dynamics in MDCK cells, we compared cells expressing GFP–MIM with neighboring non-transfected cells. Interestingly, F-actin staining was brighter at the intercellular contacts of MIM-transfected cells compared with non-transfected cells. Quantification of the F-actin intensity at the intercellular contacts (additional materials and methods; please contact the author for further information) revealed that cells expressing moderate levels of wild-type MIM displayed an ~18% increase in the amount of F-actin at cell–cell contacts compared with non-transfected cells, indicating that MIM induces actin polymerization or recruits actin filaments to cell–cell contacts. Importantly, this activity was significantly reduced when the actin-monomer-binding WH2 domain of MIM was deleted ($P<0.05$) or when the lipid-binding site was inactivated ($P<0.05$) (one-way ANOVA) (Fig. 7A–C).

Previously, MIM was shown to promote Arp2/3-mediated actin polymerization through interaction with the actin-binding protein cortactin (Lin et al., 2005). More recently, a *Drosophila* I-BAR domain protein that is related to mouse MIM and ABBA was shown to interact with this actin-binding protein to promote directional cell migration (Lin et al., 2005; Quinones et al., 2010). We thus generated a MIM construct where the previously identified cortactin-binding site was deleted (Lin et al., 2005). Surprisingly, this mutant localized normally to the adherens junctions and was as efficient in promoting actin assembly at cell–cell contacts as wild-type MIM, indicating that cortactin-binding by MIM is not essential for its ability to promote actin filament assembly in cultured MDCK cells. MIM also undergoes Src-dependent phosphorylation at Tyr397 and Tyr398. Mutation of these residues was shown to lead to a reduced dorsal ruffling by MIM, indicating the importance of MIM phosphorylation in actin remodeling (Wang, Y. et al., 2007b). However, Tyr397Phe/Tyr398Phe mutation did not display significant effects on localization of MIM to cell–cell contacts or its ability to promote actin assembly at these sites in MDCK cells (Fig. 7B,C).

To examine whether the MIM-promoted actin filament assembly is dependent on the Arp2/3 complex, we inactivated the Arp2/3 complex by expressing a Scar WA construct in MDCK cells (Machesky and Insall, 1998). This inhibited the polarization of the cells and thus studies concerning the possible interplay between MIM and Arp2/3 were carried out in non-polarized MDCK cells. Importantly, inactivation of Arp2/3 diminished MIM-induced actin assembly (supplementary material Fig. S8). Collectively, these data propose that MIM mediates Arp2/3-dependent actin filament assembly at cell–cell contacts. This activity is dependent on the intact membrane-binding I-BAR domain and actin-monomer-binding WH2 domain, but does not require MIM phosphorylation at Tyr397 or Tyr398, or its interaction with cortactin.

To further examine the role of MIM in formation and maintenance of intercellular junctions, we disrupted cadherin-based adhesion of MDCK cells by depleting Ca^{2+} with 5 mM EGTA (supplementary material Fig. S9). After 15 and 30 minutes of Ca^{2+} removal, the adhesions in non-transfected cells started to dismantle, whereas in

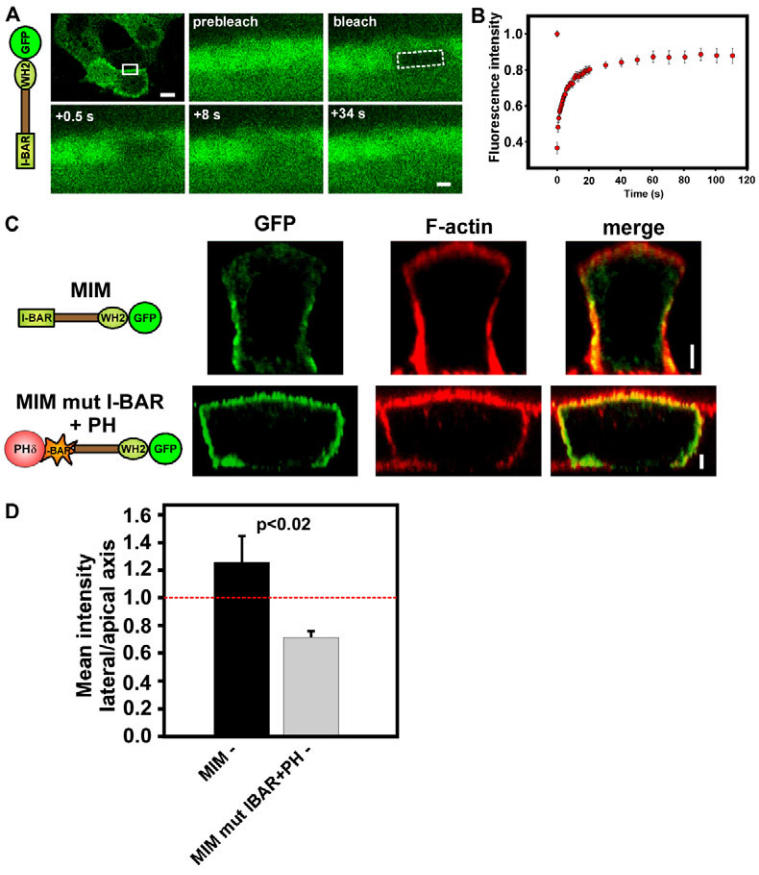

Fig. 6. MIM displays dynamic localization to intercellular junctions. (**A**) FRAP analysis of MIM–GFP dynamics at intercellular junctions of MDCK cells. Image displays a cell–cell contact area (indicated by white box in the panel in upper left corner) before and after photobleaching. Scale bars: 10 µm (top) and 1 µm (bottom). (**B**) Graph displaying the mean recovery values from nine FRAP experiments; error bars indicate s.e.m. This analysis demonstrates dynamic association ($t_{1/2}$ ~7 seconds) of GFP–MIM to cell–cell contacts. (**C**) MIM localizes preferentially to the lateral adhesion zone, whereas a MIM construct in which the I-BAR domain has been inactivated by point mutations and fused to a PtdIns(4,5)P_2-specific PH domain does not display preferential accumulation to the lateral cell–cell adhesion zone. Scale bars: 2 µm. (**D**) Quantification of the localization of MIM fusion constructs to the lateral–apical axis demonstrates that wild-type MIM preferentially localizes to the lateral domain, whereas the mutant MIM [containing an inactivated I-BAR domain fused to the PtdIns(4,5)P_2-specific PH domain] displays stronger localization to the apical surface ($P<0.02$, Mann-Whitney rank sum test). Error bars represent s.e.m.

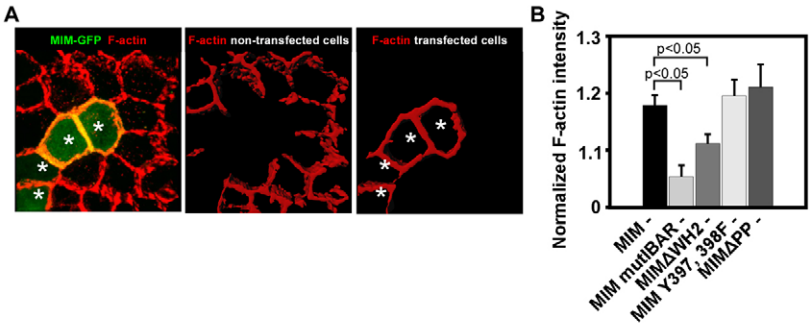

C

Biological function:	Membrane-binding/bending	Phosphorylation	Cortactin-binding	Actin monomer-binding
Reference	Mattila et al. 2007	Wang et al. 2007	Lin et al. 2005	Mattila et al. 2003
Inactivation	K146,149,150A	Y397,388F	Δ615-730	K746,747A+Δ749-759
Localization defect	yes	no	no	no
F-actin assembly defect	yes	no	no	yes

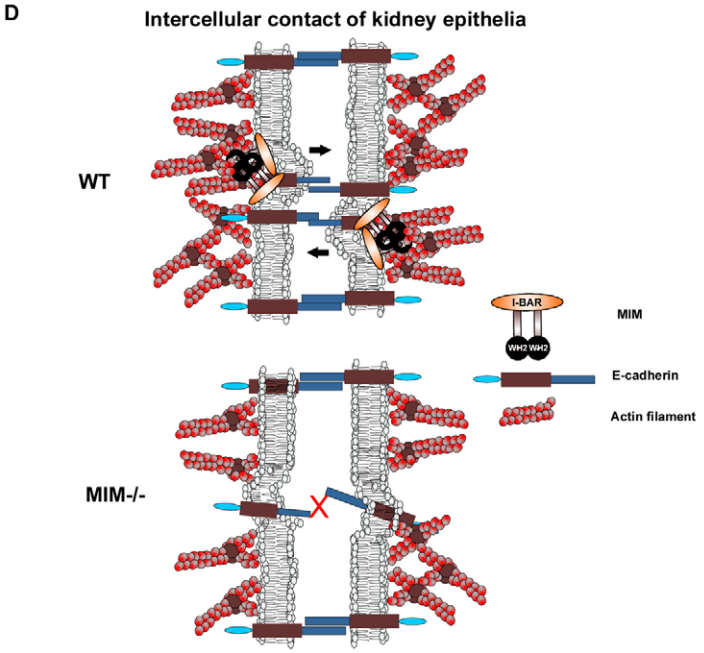

Fig. 7. MIM promotes F-actin assembly at intercellular junctions through its I-BAR and WH2 domains. (**A**) For quantification of F-actin intensity, the intercellular contacts of transfected cells (indicated by asterisks, right panel) were separated from non-transfected cells (middle panel) and the average F-actin intensity of cell–cell contacts of transfected cells was normalized to that of a non-transfected neighboring cell from the same image stack. (**B**) Average intensities of 7–23 confocal stacks were plotted on a graph and the statistical analysis was performed using one-way ANOVA. Error bars represent s.e.m. (**C**) Summary of the effects of various MIM mutations on the subcellular localization and on the ability to promote actin filament accumulation at intercellular junctions in MDCK cells. (**D**) A working model representing possible functions of MIM at the intercellular contacts of kidney epithelia. MIM senses and/or generates membrane curvature at these sites through its I-BAR domain, and promotes Arp2/3-dependent actin filament assembly through a mechanism that is at least partially dependent on the presence of an intact WH2 domain. In the absence of MIM, the intercellular junctions are compromised.

most cases, E-cadherin and phalloidin staining at the boundary between two adjacent cells expressing MIM–GFP was still prominent (supplementary material Fig. S9B,C). This suggests that MIM contributes to the stability of cadherin adhesions upon calcium removal. However, after 1 hour of Ca^{2+} depletion, the majority of both non-transfected cells and cells overexpressing MIM displayed a rounded morphology; the MIM–GFP signal was mostly cytoplasmic (supplementary material Fig. S9D). To analyze the localization of MIM–GFP during re-establishment of intercellular adhesions, we replaced the EGTA-containing medium with Ca^{2+}-containing medium and monitored the reassembly of cell–cell adhesions. Interestingly, MIM did not accumulate at newly forming adhesions and was found only in more mature adhesions along with E-cadherin (supplementary material Fig. S9F,G). Together, these data suggest that MIM is not involved in the formation of intercellular junctions, but instead contributes to their maintenance.

Discussion

MIM is a multifunctional protein that binds to actin and membranes and has been implicated in cancer metastasis (Machesky and Johnston, 2007). In addition, MIM was recently proposed to be a central component of the Shh signaling pathway (Callahan et al., 2004; Bershteyn et al., 2010). By generating and analyzing MIM-deficient mice, and by examining the localization and function of MIM in cultured cells, we show that MIM is necessary for the maintenance of cell adhesions in the kidney epithelia and provide evidence that I-BAR-domain-mediated membrane binding and WH2-domain-mediated actin-binding activities of MIM have crucial roles in this process. Surprisingly, analysis of MIM mutant mice and crossing them with Ptc-deficient mice did not provide evidence for the role of full-length MIM in Shh signaling in vivo. This conclusion is further supported by studies on an NIH3T3 cell culture model, which failed to detect any role of MIM in Shh-

induced transcription in cells. Furthermore, MIM did not interact with Gli1 or Gli2 in a co-immunoprecipitation assay. Although these data demonstrate that full-length MIM is dispensable for Shh signaling, in the future it will be important to examine whether the N-terminally truncated version of MIM (AK030533) is expressed at the protein level and could have a role in Shh signaling. In this context, it is important to note that a recent study suggested that MIM additionally contributes to Shh signaling by promoting ciliogenesis, and that this activity would depend on the C-terminal region of MIM (Bershteyn et al., 2010).

Disruption of *Mim* resulted in a progressive kidney disease in adulthood and MIM-deficient mice displayed bone abnormalities. Interestingly, a recent study identified MIM as a transcriptional target of myocyte enhancer factor 2C (MEF2C) in polycystin-dependent sensing of fluid stress. Polycystin proteins are thought to act as mechanosensors in the kidney tubules, where they respond to changes in tubular fluid flow to induce downstream signaling and expression of target genes. Consistent with our findings, this study also showed that a lack of MIM leads to late-onset histological abnormalities in the kidneys (Xia et al., 2010). Thus, it is possible that upregulation of MIM in response to fluid flow sensing by polycystins promotes the strengthening of intercellular adhesions. The bone abnormalities of MIM-deficient mice identified in our study probably represent secondary effects resulting from the kidney phenotype, because MIM expression was undetectable in developing and adult bones, and similar bone abnormalities were previously reported for other mutant animals, and human diseases resulting in kidney defects (Hoenderop et al., 2003; Hou et al., 2007; Magnusson et al., 2001). In cultured MDCK cells, MIM concentrated to adherens junctions at the cell–cell contacts, where it induced an accumulation of F-actin. FRAP analysis revealed that association of MIM to intercellular contacts is highly dynamic and similar to that reported previously for actin and many actin-binding proteins, whereas E-cadherin, which colocalizes with MIM in MDCK cells, was reported to display slower dynamics (Yamada et al., 2005).

Two distinct F-actin populations are reported to exist at epithelial cell–cell contacts (Zhang et al., 2005; Yamazaki et al., 2006). The more stable population of thin actin bundles was proposed to be generated through re-organization of pre-existing actin filaments, whereas the more dynamic pool of junctional actin, is formed by de novo actin polymerization. Furthermore, two distinct actin filament nucleation pathways have been identified at epithelial cell–cell contacts: one mediated by Arp2/3 (Kovacs et al., 2002; Yamazaki et al., 2007) and the other by the formin mDia1 (Carramusa et al., 2007). Our data suggest that MIM induces F-actin assembly at the cell–cell contacts of MDCK cells in an Arp2/3-dependent manner, and that MIM displays rapid association–dissociation dynamics at these sites. Together, these results suggest that MIM is associated with the dynamic junctional actin. Owing to the relatively specific effects of MIM deficiency on the epithelial structures in mice, we suggest that depletion of MIM causes a local defect in the organization and/or dynamics of junctional actin rather than inducing more systematic defects in the actin cytoskeleton of epithelial cells. MIM might, for example, recruit or cluster F-actin assembly factors at correct foci of intercellular junctions by sensing or generating specific membrane curvature and/or by clustering phosphoinositides (Saarikangas et al., 2009). For example, PtdIns(4,5)P_2 clustering has a positive net influence on actin filament assembly (Saarikangas et al., 2010) and regulation of membrane curvature might be important for fine-tuning actin dynamics (Lee et al., 2010; Liu et al., 2008; Takano et al., 2008). Thus, MIM-mediated actin assembly might be important for the stabilization of cadherin adhesions or in generation of membrane protrusions for the re-establishment of cadherin-based adherens junctions (Fig. 7).

Importantly, mutant MIM, which was deficient in membrane binding as a result of inactivation of the I-BAR domain, did not localize to cell–cell contacts or induce an accumulation of F-actin to intercellular junctions. Furthermore, a construct in which phosphoinositide binding by the I-BAR domain was replaced with a PtdIns(4,5)P_2-binding PH domain failed to accumulate at the cell–cell junctions. These data suggest that the I-BAR domain of MIM does not localize the protein to cell–cell contacts by simply interacting with PtdIns(4,5)P_2, but might additionally sense membrane curvature to direct the protein to the correct site of action. Additionally, a MIM construct lacking the actin-monomer-binding WH2 domain displayed a significant defect in promoting F-actin assembly compared with the wild-type MIM, although this mutant still localized to cell–cell contacts. Thus, the WH2 domain of MIM is important for its role in assembly of actin filaments at intercellular contacts, possibly by increasing the local concentration of ATP–G-actin at these sites. Together, these data suggest that a dynamic interplay between the actin cytoskeleton and plasma membrane is important for the maintenance of cell–cell junctions in epithelia.

Previous studies demonstrated that the formation of intercellular adhesions in certain epithelial cells is preceded by a zippering stage driven by filopodia-like protrusions, which make contacts with the neighboring cells to facilitate epithelial sealing (Vasioukhin et al., 2000). However, no developmental abnormalities were detected in the kidneys of *Mim*$^{-/-}$ mice. Instead, the abnormal kidney phenotype progressively developed during adulthood. It is possible that this might result from a functional redundancy between MIM and other I-BAR proteins such as IRSp53, which is also expressed in the kidney (supplementary material Fig. S4). Thus, future studies using IRSp53 (Kim et al., 2009; Sawallisch et al., 2009) and MIM double-knockout mice will be necessary to analyze whether these two proteins indeed have a redundant role in the development of the kidney epithelial structures. Alternatively, it is possible that MIM-induced actin and plasma membrane dynamics have an important role only in the regeneration of adhesive structures of kidney epithelium, or that the precise interplay between the actin cytoskeleton and plasma membrane is only required for the long-term maintenance of epithelial structures in animals.

The role of MIM in epithelial integrity might also provide an explanation for studies reporting that decreased MIM expression correlates with the metastatic potential of certain epithelial cancers (Lee et al., 2002; Ma et al., 2007; Wang, Y. et al., 2007a; Liu et al., 2010). Decreased expression of MIM in epithelial cancers could weaken the cell–cell contacts and subsequently promote epithelial–mesenchymal transition (EMT) of the cancer cells. In the future, it will be important to determine the exact mechanism by which MIM promotes actin and plasma membrane dynamics to maintain cell–cell contacts in various epithelia, and to elucidate how this activity is linked to the metastatic behavior of cancers.

Materials and Methods

Generation and maintenance of mice

The generation of the MIM targeting construct was carried out by Mu transposition (Turakainen et al., 2009). All animals were handled in strict accordance with good animal practice as defined by the relevant national and/or local animal welfare bodies, and all animal work was approved by the appropriate committee.

Phenotypic analysis

A primary systemic phenotype screen was performed at the German Mouse Clinic (GMC, http://www.mouseclinic.de) (Gailus-Durner et al., 2005).

Cell culture, light microscopic methods and luciferase reporter assay

The MIM–GFP expression plasmid and the WH2 deletion constructs were previously described (Mattila et al., 2003). The constructs for inactivation of the I-BAR domain (K146A,149A,150A) (Mattila et al., 2007), cortactin-binding region (by deleting residues 615–730) (Lin et al., 2005) and Src phosphorylation sites (Y397,398F) (Wang, Y. et al., 2007b) of MIM, and the fusion of MIM to PH domain of PLCδ domain (Varnai and Balla, 1998) were generated by PCR. The Scar W and WA constructs (Machesky and Insall, 1998) were a gift from Laura Machesky (Beatson Institute for Cancer Research, Glasgow, UK). MDCK, U2OS and NIH3T3 cells were cultured in D-MEM supplemented with 10% fetal calf serum. Shh reporter assays were performed as described (Taipale et al., 2000). Transfection of U2OS cells and quantification of filopodia was performed as described (Saarikangas et al., 2009). MDCK cells were polarized by culture for 3 days on Transwell 0.4 μm polycarbonate membrane permeable supports (Corning). Cells were transfected (day 1) using Lipofectamine 2000 (Invitrogen) following the manufacturer's guidelines and were fixed (day 3) in 4% paraformaldehyde. Cells were permeabilized with 0.3% Triton X-100 in PBS for 30 minutes, incubated with primary antibodies against E-cadherin (Transduction Laboratories) and ZO-1 (Zymed Laboratories) overnight at 4°C and with secondary antibodies for 2 hours at room temperature.

Further details of materials and methods, and any associated references can be obtained from the corresponding author.

We are grateful to R. Savolainen for the expertise in ES cell work, and E. Koivunen and A.-L. Nyfors for technical help. The Helsinki University Transgenic Animals Unit and the Viikki Laboratory Animal Centre are acknowledged for the expertise in generation and maintenance of the MIM-deficient mice. I. Thesleff, J. Pispa, J. Jernvall, and P. Munne are acknowledged for expertise in ectodermal organ analysis. J. Peränen is acknowledged for providing various antibodies and K. Tanhuanpää for help with image analysis. We thank Laura Machesky and Tamas Balla for sharing reagents. We thank the members of the German Mouse Clinic for comprehensive phenotyping of the MIM-deficient mice and fruitful discussions. We are grateful to Reinhard Seeliger, Elfi Holupirek, and Eleonore Samson and the GMC animal caretaker team for expert technical help. This study was supported by grants from the Academy of Finland (grants 121248 and 218021 to S.L., and 124137 to P.L.), Finnish National Technology Agency (TEKES) and the Finnish Cancer and Finnish Cultural Foundations. J.S. was supported by fellowships from Helsinki Graduate School in Biotechnology and Molecular Biology (GSBM), Emil Aaltonen, and Oscar Öflund Foundations. P.M. by fellowships from Viikki Graduate School in Biosciences and Alfred Kordelin, Maud Kuistila, Ida Montini, Farmos, and Biomedicum Foundations. M.V. was supported by GSBM, Paulo, Finnish Cultural, Emil Aaltonen, Wihuri, Orion-Farmos and Biomedicum Helsinki Foundations. The German Mouse Clinic received funding from the EU (EUMODIC grant LSHG-2006-037188) and the Federal Ministry of Education and Research (NGFNplus grants 01GS0851 to B.R. and E.W. and 01GS0850 to J.C.-W., M.T., W.H., M.H., H.F., V.G.-D., I.E. and M.H.A.).

Supplementary material available online at
http://jcs.biologists.org/cgi/content/full/124/8/1245/DC1

References

Bai, C. B., Auerbach, W., Lee, J. S., Stephen, D. and Joyner, A. L. (2002). Gli2, but not Gli1, is required for initial Shh signaling and ectopic activation of the Shh pathway. *Development* **129**, 4753-4761.

Bershteyn, M., Atwood, S. X., Woo, W. M., Li, M. and Oro, A. E. (2010). MIM and cortactin antagonism regulates ciliogenesis and hedgehog signaling. *Dev. Cell* **19**, 270-283.

Bompard, G., Sharp, S. J., Freiss, G. and Machesky, L. M. (2005). Involvement of Rac in actin cytoskeleton rearrangements induced by MIM-B. *J. Cell Sci.* **118**, 5393-5403.

Callahan, C. A., Ofstad, T., Horng, L., Wang, J. K., Zhen, H. H., Coulombe, P. A. and Oro, A. E. (2004). MIM/BEG4, a Sonic hedgehog-responsive gene that potentiates Gli-dependent transcription. *Genes Dev.* **18**, 2724-2729.

Carramusa, L., Ballestrem, C., Zilberman,Y. and Bershadsky, A. D. (2007). Mammalian diaphanous-related formin Dia1 controls the organization of E-cadherin-mediated cell-cell junctions. *J. Cell Sci.* **120**, 3870-3882.

Chhabra, E. S. and Higgs, H. N. (2007). The many faces of actin: matching assembly factors with cellular structures. *Nat. Cell Biol.* **9**, 1110-1121.

Doherty, G. J. and McMahon, H. T. (2008). Mediation, modulation, and consequences of membrane-cytoskeleton interactions. *Annu. Rev. Biophys.* **37**, 65-95.

Frost, A., Unger, V. M. and De Camilli, P. (2009). The BAR domain superfamily: membrane-molding macromolecules. *Cell* **137**, 191-196.

Gailus-Durner, V., Fuchs, H., Becker, L., Bolle, I., Brielmeier, M., Calzada-Wack, J., Elvert, R., Ehrhardt, N., Dalke, C., Franz, T. J. et al. (2005). Introducing the German Mouse Clinic: open access platform for standardized phenotyping. *Nat. Methods* **2**, 403-404.

Gonzalez-Quevedo, R., Shoffer, M., Horng, L. and Oro, A. E. (2005). Receptor tyrosine phosphatase-dependent cytoskeletal remodeling by the hedgehog-responsive gene MIM/BEG4. *J. Cell Biol.* **168**, 453-463.

Goodrich, L. V., Milenkovic, L., Higgins, K. M. and Scott, M. P. (1997). Altered neural cell fates and medulloblastoma in mouse patched mutants. *Science* **277**, 1109-1113.

Guerrier, S., Coutinho-Budd, J., Sassa, T., Gresset, A., Jordan, N. V., Chen, K., Jin, W. L., Frost, A. and Polleux, F. (2009). The F-BAR domain of srGAP2 induces membrane protrusions required for neuronal migration and morphogenesis. *Cell* **138**, 990-1004.

Hoenderop, J. G., van Leeuwen, J. P., van der Eerden, B. C., Kersten, F. F., van der Kemp, A. W., Merillat, A. M., Waarsing, J. H., Rossier, B. C., Vallon, V., Hummler, E. Et al. (2003). Renal Ca^{2+} wasting, hyperabsorption, and reduced bone thickness in mice lacking TRPV5. *J. Clin. Invest.* **112**, 1906-1914.

Hou, J., Shan, Q., Wang, T., Gomes, A. S., Yan, Q., Paul, D. L., Bleich, M. and Goodenough, D. A. (2007). Transgenic RNAi depletion of claudin-16 and the renal handling of magnesium. *J. Biol. Chem.* **282**, 17114-17122.

Itoh, T., Erdmann, K. S., Roux, A., Habermann, B., Werner, H. and De Camilli, P. (2005). Dynamin and the actin cytoskeleton cooperatively regulate plasma membrane invagination by BAR and F-BAR proteins. *Dev. Cell* **9**, 791-804.

Kim, M. H., Choi, J., Yang, J., Chung, W., Kim, J. H., Paik, S. K., Kim, K., Han, S., Won, H., Bae, Y. S. et al. (2009). Enhanced NMDA receptor-mediated synaptic transmission, enhanced long-term potentiation, and impaired learning and memory in mice lacking IRSp53. *J. Neurosci.* **29**, 1586-1595.

Kovacs, E. M., Goodwin, M., Ali, R. G., Paterson, A. D. and Yap, A. (2002). Cadherin-directed actin assembly: E-cadherin physically associates with the Arp2/3 complex to direct actin assembly in nascent adhesive contacts. *Curr. Biol.* **12**, 379-382.

Krishnan, R., Eley, L. and Sayer, J. A. (2008). Urinary concentration defects and mechanisms underlying nephronophthisis. *Kidney Blood Press. Res.* **31**, 152-162.

Lee, K., Gallop, J. L., Rambani, K. and Kirschner, M. W. (2010). Self-assembly of filopodia-like structures on supported lipid bilayers. *Science* **329**, 1341-1345.

Lee, S. H., Kerff, F., Chereau, D., Ferron, F., Klug, A. and Dominguez, R. (2007). Structural basis for the actin-binding function of missing-in-metastasis. *Structure* **15**, 145-155.

Lee, Y. G., Macoska, J. A., Korenchuk, S. and Pienta, K. J. (2002). MIM, a potential metastasis suppressor gene in bladder cancer. *Neoplasia* **4**, 291-294.

Lin, J., Liu, J., Wang, Y., Zhu, J., Zhou, K., Smith, N. and Zhan, X. (2005). Differential regulation of cortactin and N-WASP-mediated actin polymerization by missing in metastasis (MIM) protein. *Oncogene* **24**, 2059-2066.

Liu, A. P., Richmont, D. L., Maibaum, L., Pronk, S., Geissler, P. L. and Fletcher, D. A. (2008). Membrane-induced bundling of actin filaments. *Nat. Phys.* **4**, 789-793.

Liu, K., Wang, G., Ding, H., Chen, Y. and Wang, J. (2010). Downregulation of metastasis suppressor (MTSS1) is associated with nodal metastasis and poor outcome in Chinese patients with gastric cancer. *BMC Cancer* **10**, 428.

Ma, S., Guan, X. Y., Lee, T. K. and Chan, K. W. (2007). Clinicopathological significance of missing in metastasis B expression in hepatocellular carcinoma. *Hum. Pathol.* **38**, 1201-1206.

Machesky, L. M. and Insall, R. H. (1998). Scar1 and the related Wiskott-Aldrich syndrome protein, WASP, regulate the actin cytoskeleton through the Arp2/3 complex. *Curr. Biol.* **8**, 1347-1356.

Machesky, L. M. and Johnston, S. A. (2007). MIM: a multifunctional scaffold protein. *J. Mol. Med.* **85**, 569-576.

Magnusson, P., Sharp, C. A., Magnusson, M., Risteli, J., Davie, M. W. and Larsson, L. (2001). Effect of chronic renal failure on bone turnover and bone alkaline phosphatase isoforms. *Kidney Int.* **60**, 257-265.

Massari, S., Perego, C., Padovano, V., D'Amico, A., Raimondi, A., Francolini, M. and Pietrini, G. (2009). LIN7 mediates the recruitment of IRSp53 to tight junctions. *Traffic* **10**, 246-257.

Mattila, P. K., Salminen, M., Yamashiro, T. and Lappalainen, P. (2003). Mouse MIM, a tissue-specific regulator of cytoskeletal dynamics, interacts with ATP-actin monomers through its C-terminal WH2 domain. *J. Biol. Chem.* **278**, 8452-8459.

Mattila, P. K., Pykalainen, A., Saarikangas, J., Paavilainen, V. O., Vihinen, H., Jokitalo, E. and Lappalainen, P. (2007). Missing-in-metastasis and IRSp53 deform PI(4,5)P2-rich membranes by an inverse BAR domain-like mechanism. *J. Cell Biol.* **176**, 953-964.

Peter, B. J., Kent, H. M., Mills, I. G., Vallis, Y., Butler, P. J., Evans, P. R. and McMahon, H. T. (2004). BAR domains as sensors of membrane curvature: the amphiphysin BAR structure. *Science* **303**, 495-499.

Quinones, G. A., Jin, J. and Oro, A. E. (2010). I-BAR antagonism of endocytosis mediates directional sensing during guided cell migration. *J. Cell Biol.* **189**, 353-367.

Saarikangas, J., Hakanen, J., Mattila, P. K., Grumet, M., Salminen, M.,and Lappalainen, P. (2008). ABBA regulates plasma-membrane and actin dynamics to promote radial glia extension. *J. Cell Sci.* **121**, 1444-1454.

Saarikangas, J., Zhao, H., Pykalainen, A., Laurinmaki, P., Mattila, P. K., Kinnunen, P. K., Butcher, S. J. and Lappalainen, P. (2009). Molecular mechanisms of membrane deformation by I-BAR domain proteins. *Curr. Biol.* **19**, 95-107.

Saarikangas, J., Zhao, H. and Lappalainen, P. (2010). Regulation of the actin cytoskeleton-plasma membrane interplay by phosphoinositides. *Physiol. Rev.* **90**, 259-289.

Sawallisch, C., Berhorster, K., Disanza, A., Mantoani, S., Kintscher, M., Stoenica, L., Dityatev, A., Sieber, S., Kindler, S., Morellini, F. et al. (2009). The insulin receptor substrate of 53 kDa (IRSp53) limits hippocampal synaptic plasticity. *J. Biol. Chem.* **284**, 9225-9236.

Scita, G., Confalonieri, S., Lappalainen, P. and Suetsugu, S. (2008). IRSp53: crossing the road of membrane and actin dynamics in the formation of membrane protrusions. *Trends Cell Biol.* **18**, 52-60.

Simon, D. B., Lu, Y., Choate, K. A., Velazquez, H., Al-Sabban, E., Praga, M., Casari, G., Bettinelli, A., Colussi, G., Rodriguez-Soriano, J. et al. (1999). Paracellin-1, a renal tight junction protein required for paracellular Mg^{2+} resorption. *Science* **285**, 103-106.

Suetsugu, S., Murayama, K., Sakamoto, A., Hanawa-Suetsugu, K., Seto, A., Oikawa, T., Mishima, C., Shirouzu, M., Takenawa, T. and Yokoyama, S. (2006).The RAC binding domain/IRSp53-MIM homology domain of IRSp53 induces RAC-dependent membrane deformation. *J. Biol. Chem.* **281**, 35347-35358.

Taipale, J., Chen, J. K., Cooper, M. K., Wang, B., Mann, R. K., Milenkovic, L., Scott, M. P. and Beachy, P. A. (2000). Effects of oncogenic mutations in Smoothened and Patched can be reversed by cyclopamine. *Nature* **406**, 1005-1009.

Takano, K., Toyooka, K. and Suetsugu, S. (2008). EFC/F-BAR proteins and the N-WASP-WIP complex induce membrane curvature-dependent actin polymerization. *EMBO J.* **27**, 2817-2828.

Turakainen, H., Saarimaki-Vire, J., Sinjushina, N., Partanen, J. and Savilahti, H. (2009). Transposition-based method for the rapid generation of gene-targeting vectors to produce Cre/Flp-modifiable conditional knock-out mice. *PLoS One* **4**, e4341.

Varjosalo, M. and Taipale, J. (2008). Hedgehog: functions and mechanisms. *Genes Dev.* **22**, 2454-2472.

Varnai, P. and Balla, T. (1998). Visualization of phosphoinositides that bind pleckstrin homology domains: calcium- and agonist-induced dynamic changes and relationship to myo-[3H]inositol-labeled phosphoinositide pools. *J. Cell Biol,* **143**, 501-510.

Vasioukhin, V., Bauer, C., Yin, M. and Fuchs, E. (2000). Directed actin polymerization is the driving force for epithelial cell-cell adhesion. *Cell* **100**, 209-219.

Wang, W., Eddy, R. and Condeelis, J. (2007a). The cofilin pathway in breast cancer invasion and metastasis. *Nat. Rev. Cancer* **7**, 429-440.

Wang, W., Soltero, L., Zhang, P., Huang, X. R., Lan, H. Y. and Adrogue, H. J. (2007b). Renal inflammation is modulated by potassium in chronic kidney disease: possible role of Smad7. *Am. J. Physiol. Renal Physiol.* **293**, F1123-F1130.

Wang, Y., Liu, J., Smith, E., Zhou, K., Liao, J., Yang, G. Y., Tan, M. and Zhan, X. (2007a). Downregulation of Missing in Metastasis Gene (MIM) is associated with the progression of bladder transitional carcinomas. *Cancer Invest.* **25**, 79-86.

Wang, Y., Zhou, K., Zeng, X., Lin, J. and Zhan, X. (2007b). Tyrosine phosphorylation of missing in metastasis protein is implicated in platelet-derived growth factor-mediated cell shape changes. *J. Biol. Chem.* **282**, 7624-7631.

Woodings, J. A., Sharp, S. J. and Machesky, L. M. (2003). MIM-B, a putative metastasis suppressor protein, binds to actin and to protein tyrosine phosphatase delta. *Biochem. J.* **371**, 463-471.

Xia, S., Li, X., Johnson, T., Seidel, C., Wallace, D. P. and Li, R. (2010). Polycystin-dependent fluid flow sensing targets histone deacetylase 5 to prevent the development of renal cysts. *Development* **137**, 1075-1084.

Yamada, S., Pokutta, S., Drees, F., Weis, W. I. and Nelson, W. J. (2005). Deconstructing the cadherin-catenin-actin complex. *Cell* **123**, 889-901.

Yamagishi, A., Masuda, M., Ohki, T., Onishi, H. and Mochizuki, N. (2004). A novel actin bundling/filopodium-forming domain conserved in insulin receptor tyrosine kinase substrate p53 and missing in metastasis protein. *J. Biol. Chem.* **279**, 14929-14936.

Yamazaki, D., Oikawa, T. and Takenawa, T. (2007). Rac-WAVE-mediated actin reorganization is required for organization and maintenance of cell-cell adhesion. *J. Cell Sci.* **120**, 86-100.

Zhang, J., Betson, M., Erasmus, J., Zeikos, K., Bailly, M., Cramer, L. P. and Braga, V. M. M. (2005). Actin at cell-cell junctions is composed of two dynamic and functional populations. *J. Cell Sci.* **188**, 5549-5562.